Supporting Information

Atomic Layer Deposition of Molybdenum and Tungsten Oxide Thin Films using Heteroleptic Imido-Amidinato precursors: Process Development, Film Characterization, and Gas Sensing Properties

Miika Mattinen,*† Jan-Lucas Wree,‡ Niklas Stegmann,‡ Engin Ciftyurek,¥ Mhamed El Achhab,¥ Peter J. King,† Kenichiro Mizohata,§ Jyrki Räisänen,§ Klaus D. Schierbaum,¥ Anjana Devi,‡ Mikko Ritala,*† Markku Leskelä†

† Department of Chemistry, University of Helsinki, P.O. Box 55, 00014, Finland

‡ Inorganic Materials Chemistry, Faculty of Chemistry and Biochemistry, Ruhr-University Bochum, Universitätsstr. 150, 44801 Bochum, Germany

¥ Material Science Department, Institute of Experimental Condensed Matter Physics, Heinrich Heine University Düsseldorf, Universitätsstr. 1, 40225, Düsseldorf, Germany

§ Division of Materials Physics, Department of Physics, University of Helsinki, P.O. Box 43, 00014, Finland

*E-mail: miika.mattinen@helsinki.fi

*E-mail: mikko.ritala@helsinki.fi

Contents

1. Film growth and thickness measurements by different methods S2
2. Conformality S5
3. MoO_x films deposited at different temperatures S6
4. MoO_x films of different thicknesses deposited at 300 °C S8
5. Effects of $[Mo(N^tBu)_2(dpamd)_2]$ and O_3 pulses S9
6. WO_x films deposited at different temperatures S12
7. WO_x films of different thicknesses deposited at 300 °C S13
8. Effects of $[W(N^tBu)_2(dpamd)_2]$ and O_3 pulses S14
9. XPS of MoO_x films S17
10. Characterization of 50 nm MoO_x films used for resistivity and gas sensor measurements S18

References S19

1. Film growth and thickness measurements by different methods

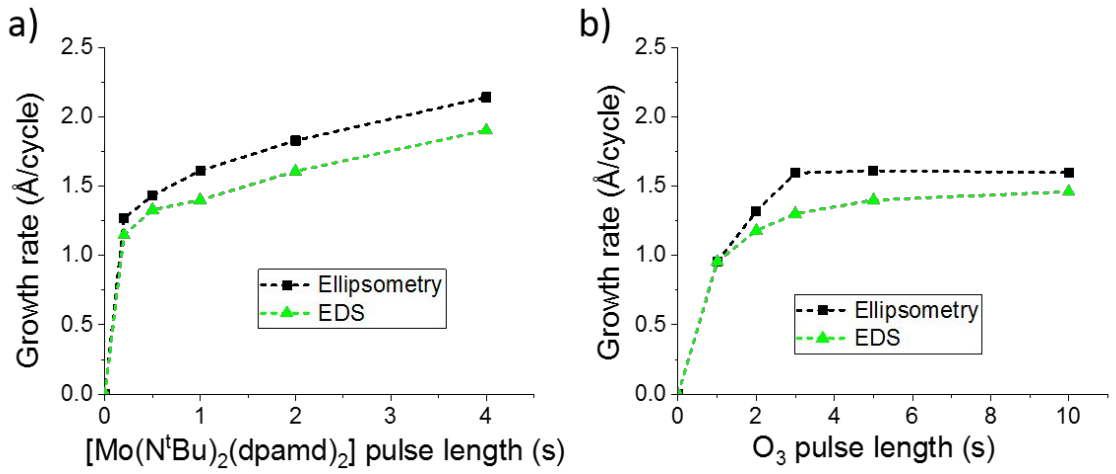

Figure S1 Growth rates of MoO_x films deposited using different a) $[Mo(N^tBu)_2(dpamd)_2]$ and b) O_3 pulse lengths at 300 °C as measured by ellipsometry and EDS. Unless otherwise noted, the films were deposited using 1000 cycles with 1 s $[Mo(N^tBu)_2(dpamd)_2]$ and 5 s O_3 pulses. XRR could not be used due to high roughness of the films. The dashed lines are meant to guide the eye.

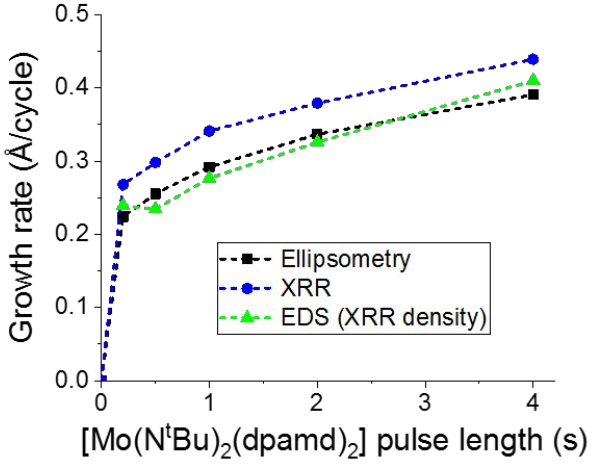

Figure S2 Growth rates of MoO_x films deposited using different $[Mo(N^tBu)_2(dpamd)_2]$ pulse lengths at 250 °C using 1000 cycles and 5 s O_3 pulses as measured by ellipsometry, EDS (using XRR density), and XRR. The dashed lines are meant to guide the eye.

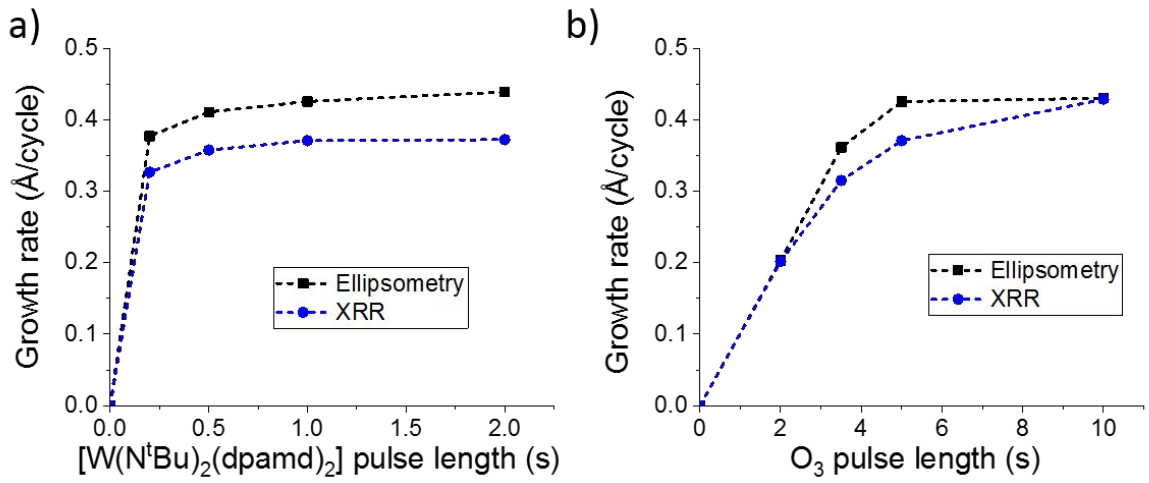

Figure S3 Growth rates of WO_x films grown at 300 °C using different a) $[W(N^tBu)_2(dpamd)_2]$ and b) O_3 pulse lengths as measured by ellipsometry and XRR. Unless otherwise noted, the films were deposited using 1000 cycles with 1 s $[W(N^tBu)_2(dpamd)_2]$ and 5 s O_3 pulses. The dashed lines are meant to guide the eye.

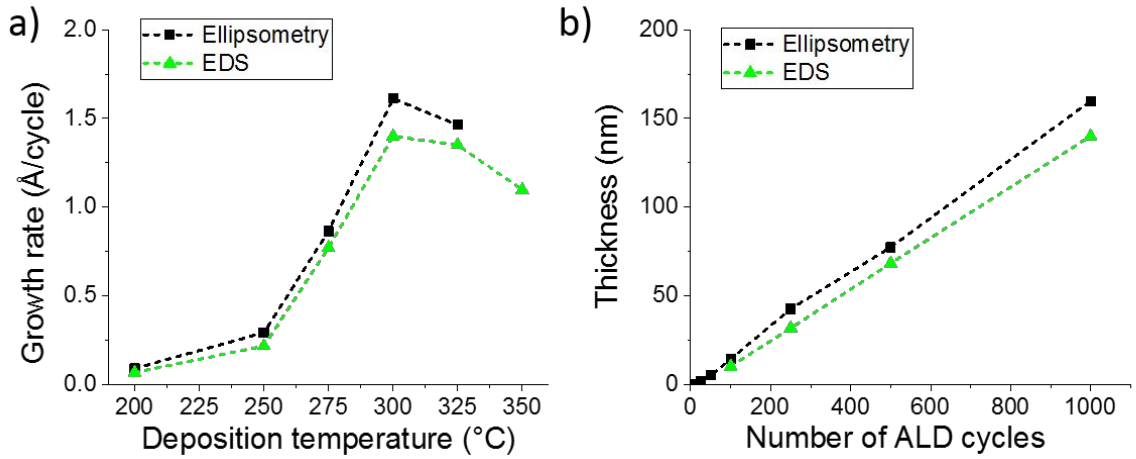

Figure S4 a) Growth rates of MoO_x films deposited at different temperatures and b) thicknesses of MoO_x films deposited with a different number of ALD cycles as measured by ellipsometry and EDS. Unless otherwise noted, the films were deposited at 300 °C using 1000 cycles with 1 s $[Mo(N^tBu)_2(dpamd)_2]$ and 5 s O_3 pulses separated by 1 s purges. The dashed lines are meant to guide the eye.

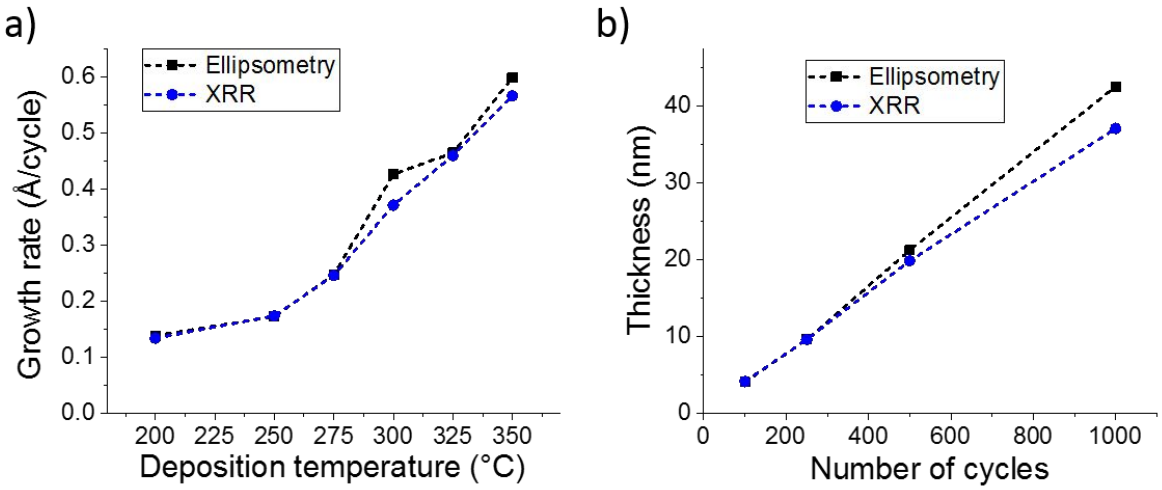

Figure S5 a) Growth rates of WO_x films deposited at different temperatures and b) thicknesses of WO_x films deposited with a different number of ALD cycles as measured by ellipsometry and XRR. Unless otherwise noted, the films were deposited at 300 °C using 1000 cycles with 1 s $[W(N^tBu)_2(dpamd)_2]$ and 5 s O_3 pulses separated by 1 s purges. The dashed lines are meant to guide the eye.

2. Conformality

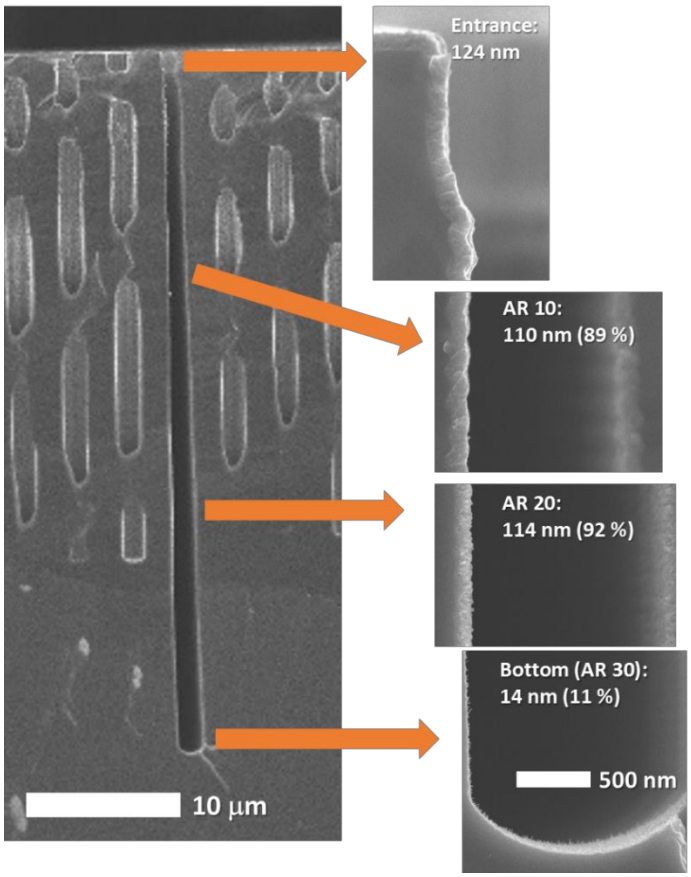

Figure S6 Cross-sectional SEM images of a MoO_x film deposited in a trench (aspect ratio 30:1). The insets show film thicknesses at aspect ratios (ARs) 0 (entrance), 10, 20, and 30 (bottom). The film was deposited at 300 °C using 750 cycles with 1 s $[Mo(N^tBu)_2(dpamd)_2]$ and 5 s O_3 pulses separated by 3 s purges. The small film thickness at the very bottom of the trench is likely due to insufficient precursor doses used in the experiment.

3. MoO_x films deposited at different temperatures

Raman spectra of the films deposited at 300 and 325 °C showed several modes attributed to α-MoO_3 when either a 532 or a 633 nm laser was used (Figure S7, see also the peak list and assignments in Table S1).[1–4] The spectrum of the film deposited at 275 °C measured with a 532 nm laser was rather featureless except for broad and weak peaks around 680, 815, and 863 cm^{-1}, as well as peaks originating from the silicon substrate (Figure S7a). Using a 633 nm laser instead resulted in broad features at approximately 280, 483, and 818 cm^{-1} for the film deposited at 275 °C (Figure S7b). The peak positions of the film deposited at 275 °C do not match those reported for α[1–4] or β[4,5] MoO_3, γ or η-Mo_4O_{11},[6–8] Mo_8O_{23},[8] or $Mo_{18}O_{52}$.[8] We are not aware of reports of Raman spectra of other suboxide phases. Instead, the shape and position of the Raman features of the 275 °C film match those reported for amorphous MoO_3,[9] suggesting that the film was not completely crystalline, and that the suboxide phase detected by XRD is not strongly Raman active.

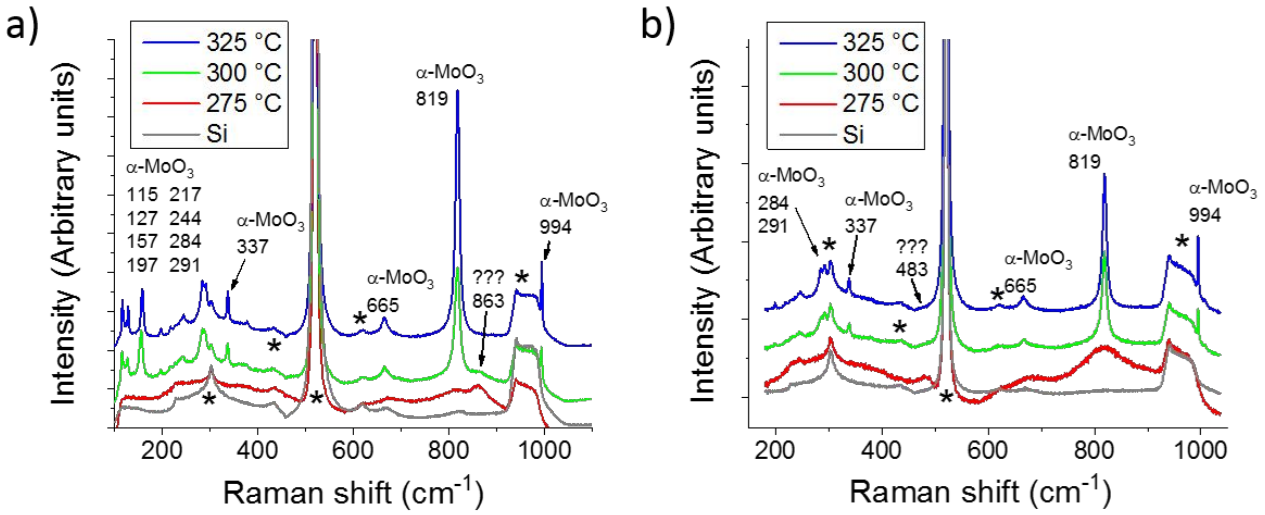

Figure S7 Raman spectra of MoO_x films deposited at different temperatures (1000 cycles) measured using a) 532 nm amd b) 633 nm laser. The peaks marked with asterisks originate from the Si substrate.

Table S1 Observed α-MoO_3 Raman modes and their assignments according to refs.1–4

Raman shift (cm^{-1})	Assignment
994	A_{1g}, B_{1g} ν(OMo)
819	B_{1g} ν(OMo_2)
665	B_{3g} ν(OMo_3)
337	A_g δ(OMo_3)
291	B_{3g} δ(OMo)
284	B_{3g} δ(OMo)
244	B_{3g} δ(OMo_2)
217	A_g δ(OMo_2)
197	B_{2g} δ(OMo_2)
157	A_g δ$(O_2Mo_2)_n$
127	B_{2g}
115	B_{1g}

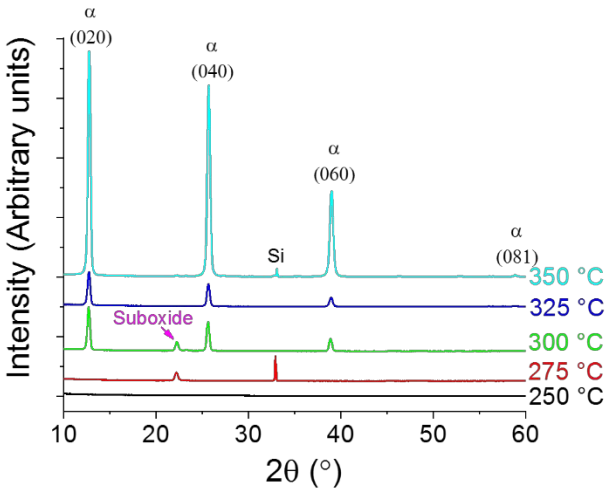

Figure S8 θ-2θ X-ray diffractograms of MoO_x films deposited at different temperatures using 1000 cycles. α refers to α-MoO_3 (PDF 005-0508).

4. MoO_x films of different thicknesses deposited at 300 °C

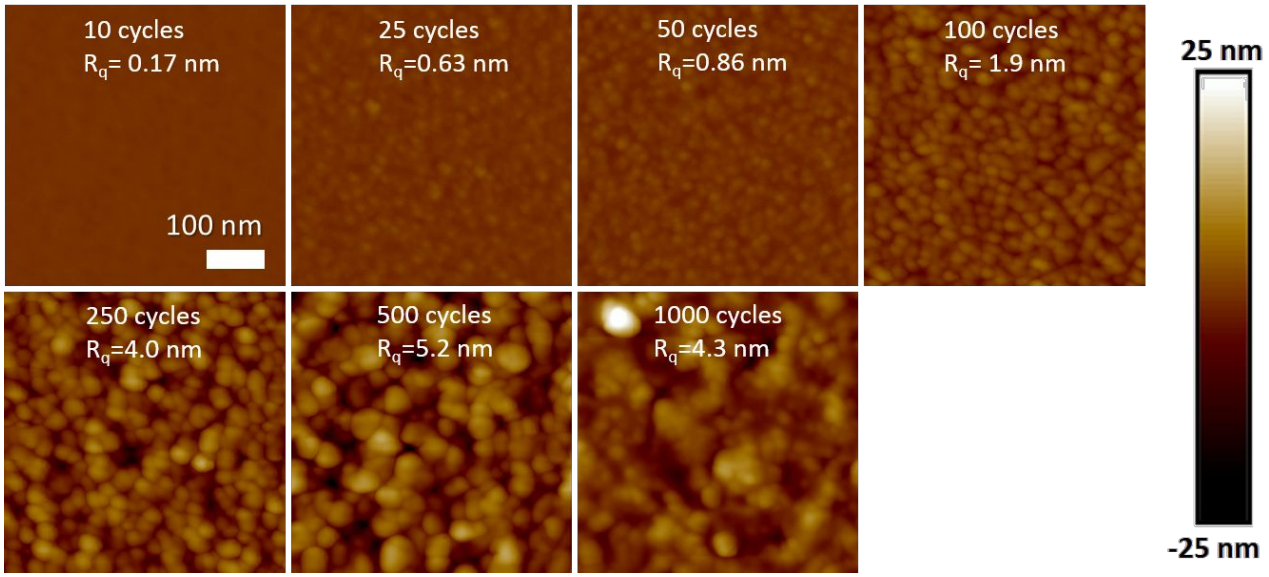

Figure S9 AFM images and roughness values (R_q) of MoO_x films deposited at 300 °C with different number of ALD cycles.

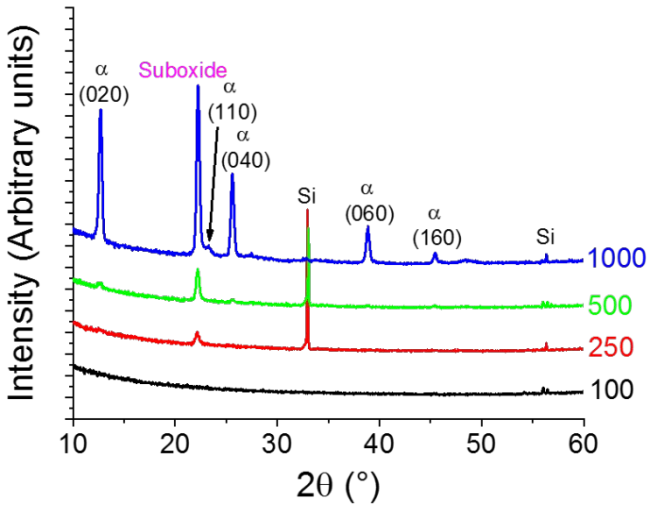

Figure S10 θ-2θ X-ray diffractograms of MoO_x films deposited at 300 °C with different number of cycles. α refers to α-MoO_3 (PDF 005-0508).

5. Effects of $[Mo(N^tBu)_2(dpamd)_2]$ and O_3 pulses

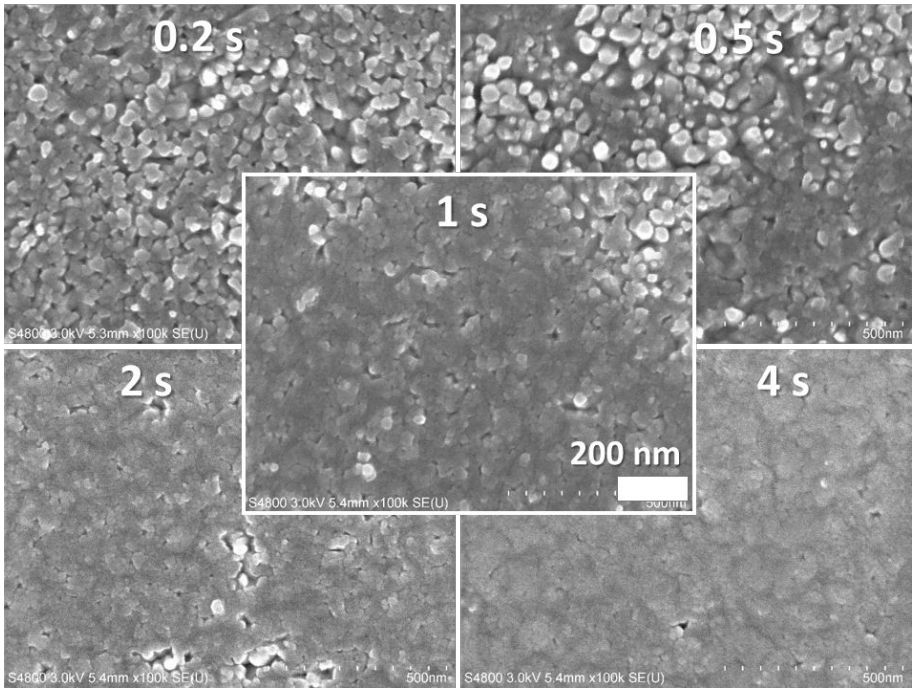

Figure S11 SEM images of MoO_x films deposited with different $[Mo(N^tBu)_2(dpamd)_2]$ pulse lengths at 300 °C using 1000 cycles with 5 s O_3 pulses.

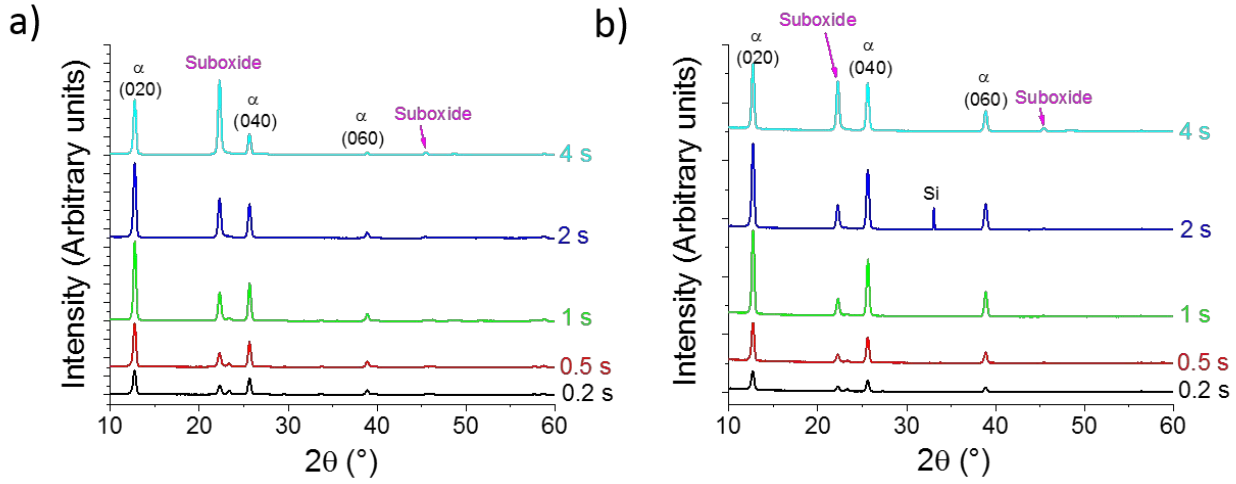

Figure S12 a) Grazing incidence and b) θ-2θ X-ray diffractograms of MoO_x films deposited with different $[Mo(N^tBu)_2(dpamd)_2]$ pulse lengths at 300 °C using 1000 cycles with 5 s O_3 pulses. α refers to α-MoO_3 (PDF 005-0508).

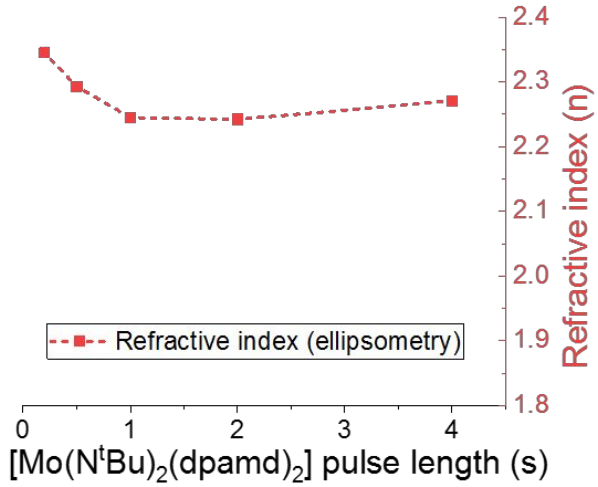

Figure S13 Refractive indices (ellipsometry, at 630 nm) of MoO_x films deposited with different $[Mo(N^tBu)_2(dpamd)_2]$ pulse lengths. Films were deposited at 300 °C using 1000 cycles and 5 s O_3 pulses. The dashed line is meant to guide the eye.

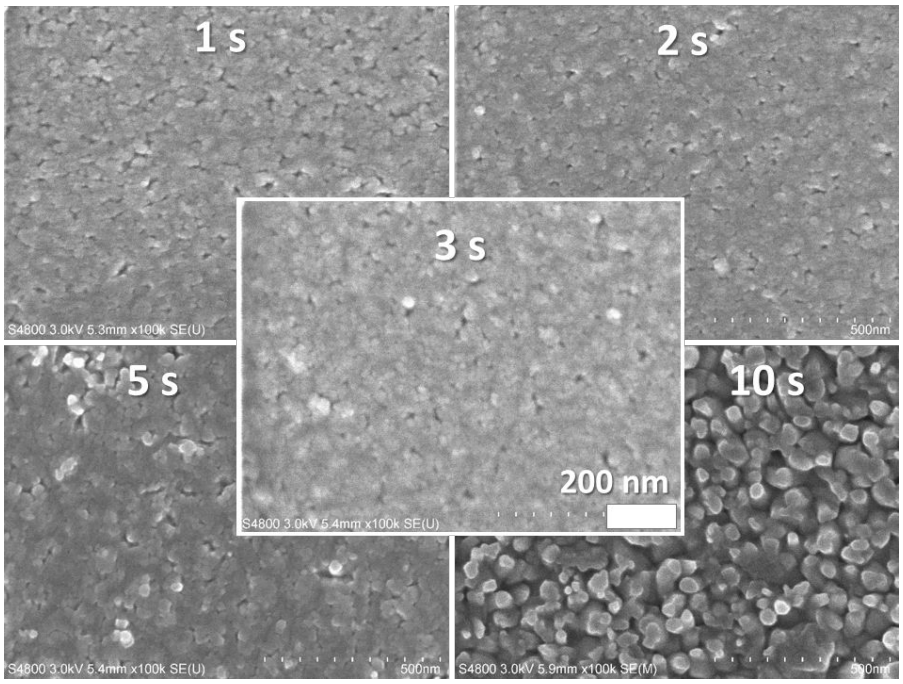

Figure S14 a) SEM images of MoO_x films deposited with different O_3 pulse lengths at 300 °C using 1000 cycles with 1 s $[Mo(N^tBu)_2(dpamd)_2]$ pulses.

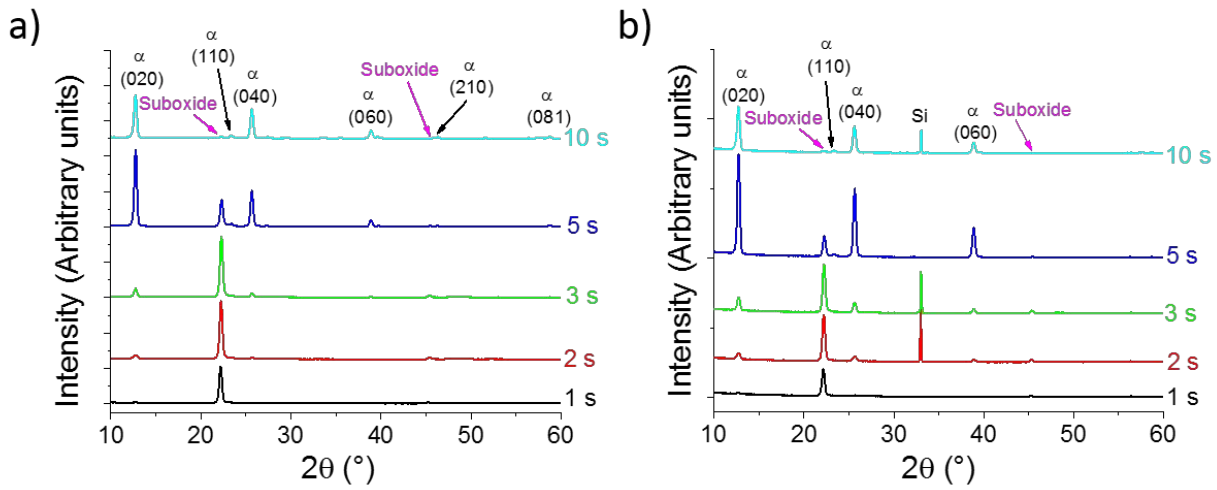

Figure S15 a) Grazing incidence and b) θ-2θ X-ray diffractograms of MoO_x films deposited with different O_3 pulse lengths at 300 °C using 1000 cycles with 1 s [$Mo(N^tBu)_2(dpamd)_2$] pulses. α refers to α-MoO_3 (PDF 005-0508).

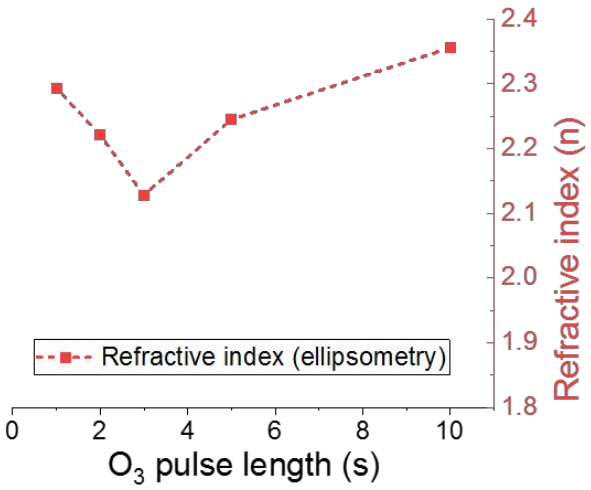

Figure S16 Refractive indices (ellipsometry, at 630 nm) of MoO_x films deposited with different O_3 pulse lengths. Films were deposited at 300 °C using 1000 cycles and 1 s [$Mo(N^tBu)_2(dpamd)_2$] pulses. The dashed line is meant to guide the eye.

6. WO_x films deposited at different temperatures

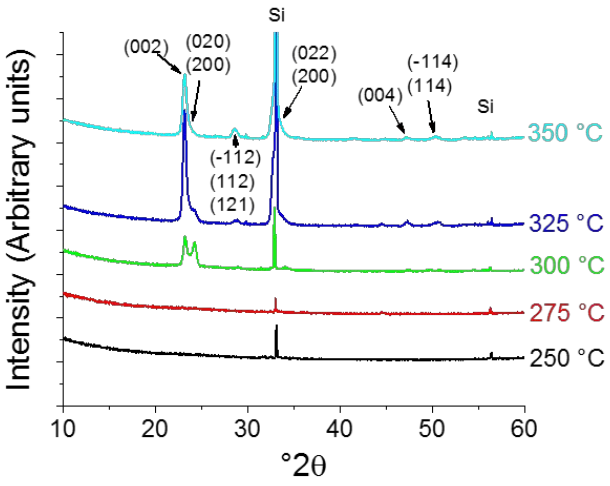

Figure S17 θ-2θ X-ray diffractograms of WO_x films deposited at different temperatures using 1000 cycles. The Miller indices refer to monoclinic γ-WO_3 (PDF 043-1035).

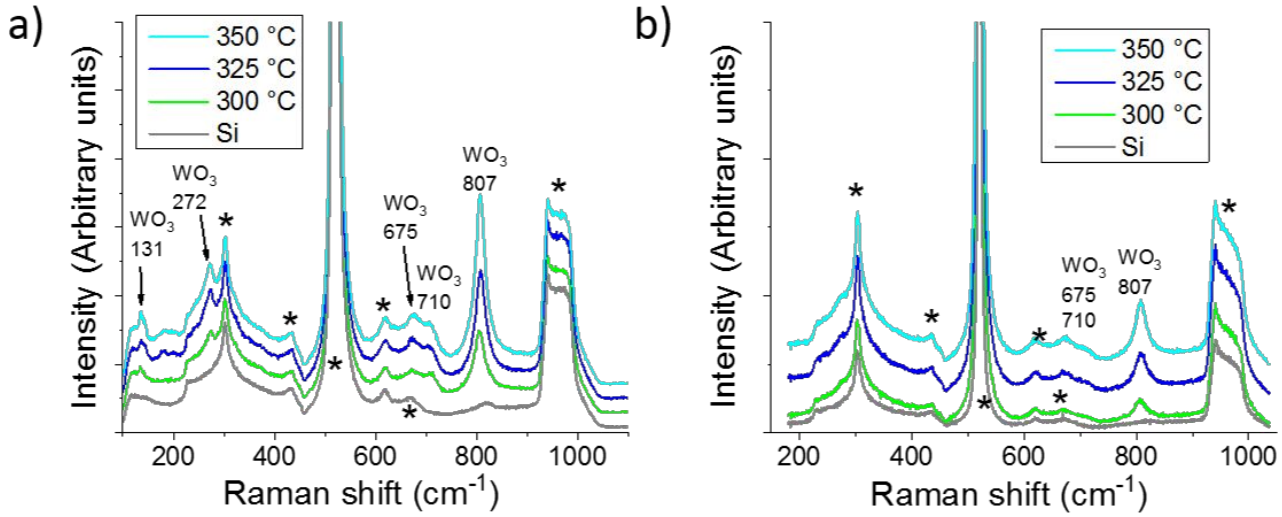

Figure S18 Raman spectra of WO_x films deposited at different temperatures (1000 cycles) measured using a) 532 nm and b) 633 nm laser. The peaks marked with asterisks originate from the Si substrate.

Table S2 Observed WO_3 Raman modes and their assignments according to refs.10,11

Raman shift (cm^{-1})	Assignment
807	ν(O-W-O)
710	ν(O-W-O)
675	γ(O-W-O)
272	δ(O-W-O)
131	lattice mode

7. WO_x films of different thicknesses deposited at 300 °C

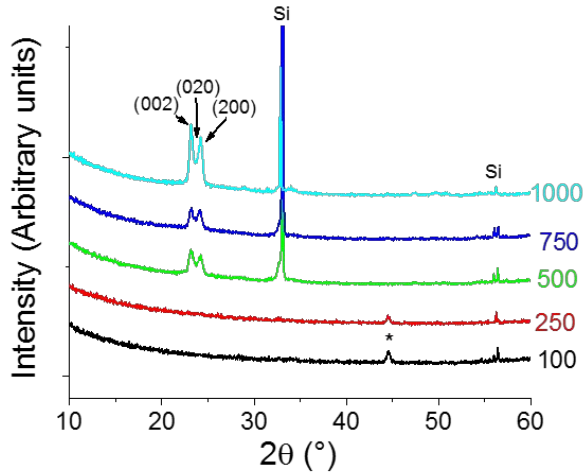

Figure S19 θ-2θ X-ray diffractograms of WO_x films deposited with different number of ALD cycles at 300 °C. The Miller indices refer to monoclinic γ-WO_3 (PDF 043-1035). The peak marked with an asterisk originates from the sample stage.

8. Effects of $[W(N^tBu)_2(dpamd)_2]$ and O_3 pulses

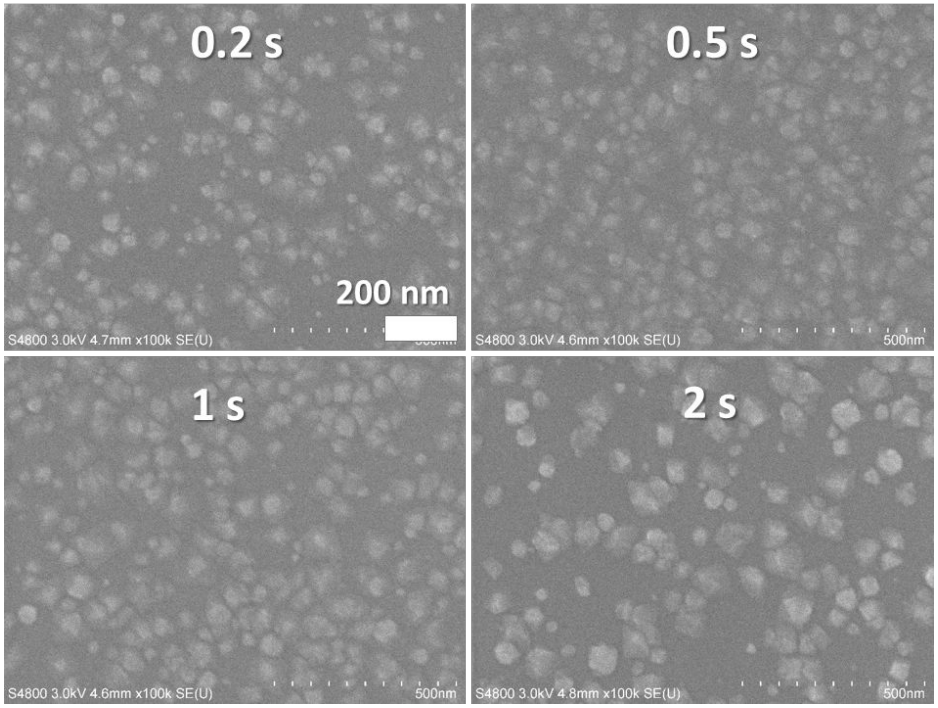

Figure S20 SEM images of WO_x films deposited with different $[W(N^tBu)_2(dpamd)_2]$ pulse lengths at 300 °C using 1000 cycles.

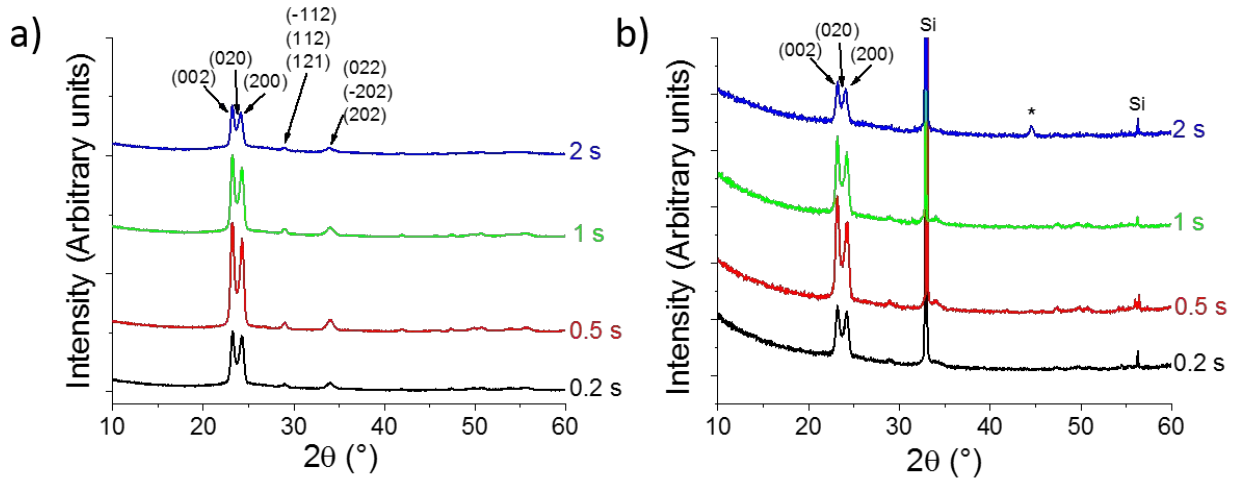

Figure S21 a) Grazing incidence and b) θ-2θ X-ray diffractograms of WO_x films deposited with different $[W(N^tBu)_2(dpamd)_2]$ pulse lengths at 300 °C using 1000 cycles. The peak marked with an asterisk originates from the sample stage.

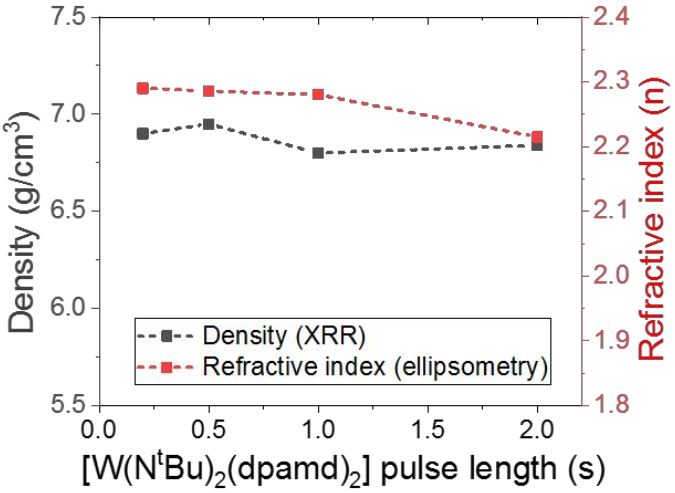

Figure S22 Densities (XRR) and refractive indices (ellipsometry, at 630 nm) of WO_x films deposited with different [$W(N^tBu)_2(dpamd)_2$] pulse lengths. Films were deposited at 300 °C using 1000 cycles and 5 s O_3 pulses. The dashed lines are meant to guide the eye.

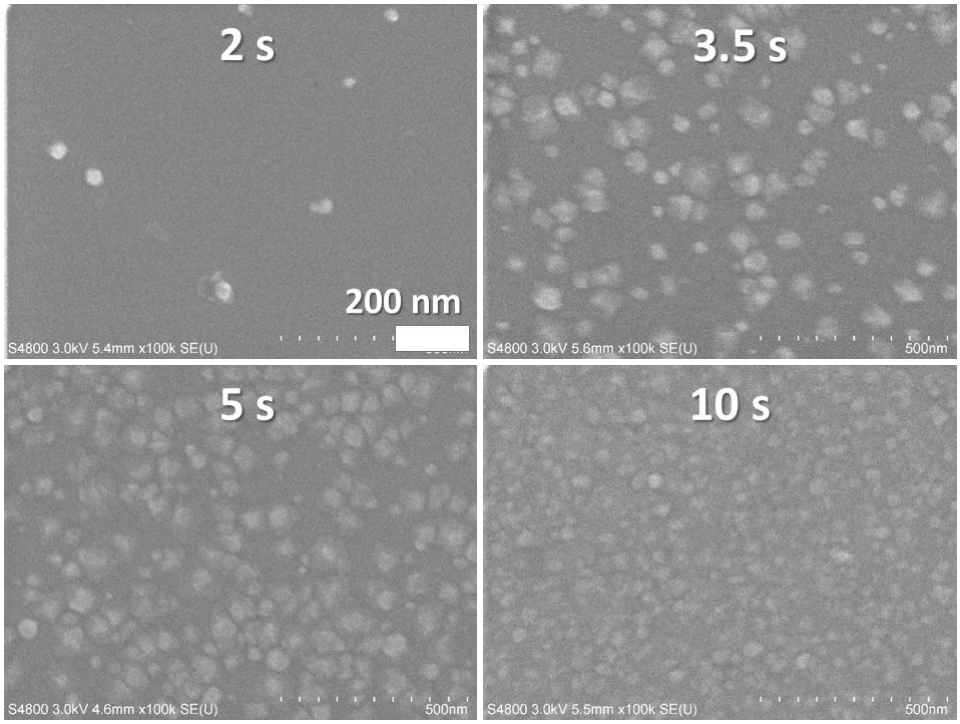

Figure S23 SEM images of WO_x films deposited with different O_3 pulse lengths at 300 °C using 1000 cycles with 1 s [$W(N^tBu)_2(dpamd)_2$] pulses.

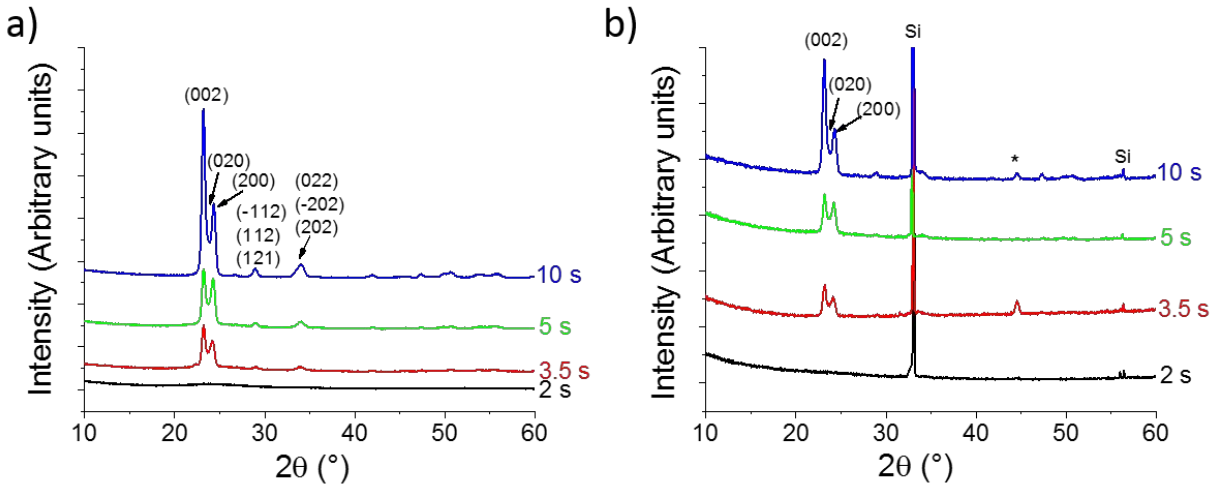

Figure S24 a) Grazing incidence and b) θ-2θ X-ray diffractograms of WO_x films deposited with different O_3 pulse lengths at 300 °C using 1000 cycles with 1 s [$W(N^tBu)_2(dpamd)_2$] pulses. The peak marked with an asterisk originates from the sample stage.

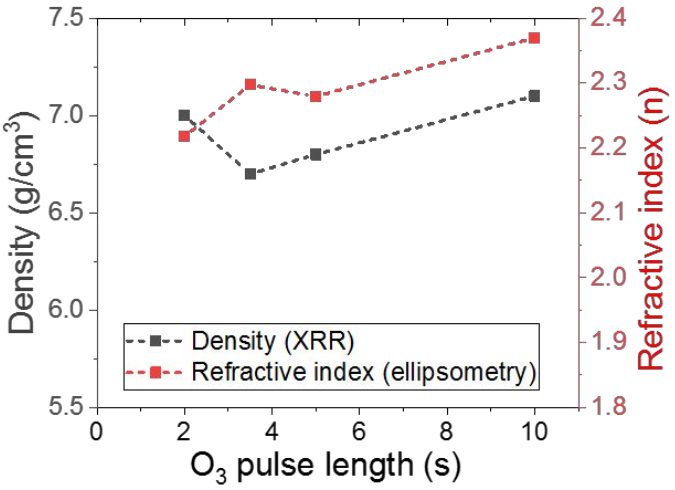

Figure S25 Densities (XRR) and refractive indices (ellipsometry, at 630 nm) of WO_x films deposited with different O_3 pulse lengths. Films were deposited at 300 °C using 1000 cycles and 1 s [$W(N^tBu)_2(dpamd)_2$] pulses. The dashed lines are meant to guide the eye.

9. XPS of MoO_x films

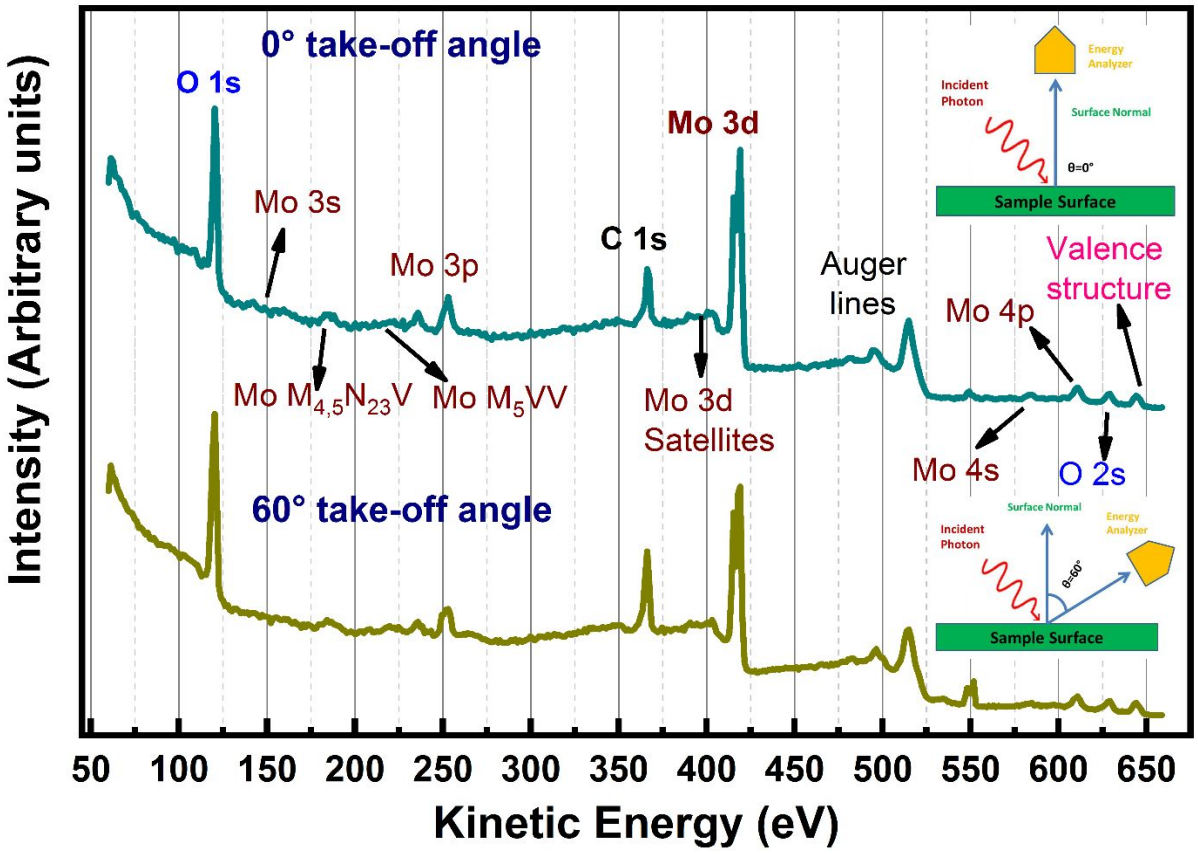

Figure S26 Photoelectron survey spectra measured with 0 and 60° take-off angles of a 50 nm MoO_x film deposited at 275 °C. The spectra were mere measured with 650 eV radiation.

Table S3 Mo $3d_{5/2}$ and O 1s binding energies, composition and work functions measured with 0 and 60° take-off angles for a 50 nm MoO_x film deposited at 275 °C

Electron take off angle (°)	Mo $3d_{5/2}$ binding energy (eV) and concentrations (at.%)			Average Mo oxidation state	Stoichiometry (O/Mo ratio)	O 1s Binding Energy (eV)					Work function (Φ) [eV]
	Mo^{4+}	Mo^{5+}	Mo^{6+}			H_2O	OH^-	O^{2-} in Mo^{4+}	O^{2-} in Mo^{5+}	O^{2-} in Mo^{6+}	
0	230.19 (21.0)	231.57 (51.0)	232.98 (28.0)	+5.1	2.6	534.37	533.71	532.77	531.49	530.55	5.98
60	230.51 (39.1)	232.01 (43.4)	233.51 (17.5)	+4.8	2.4	534.13	533.67	532.64	531.63	530.83	7.01

10. Characterization of 50 nm MoO_x films used for resistivity and gas sensor measurements

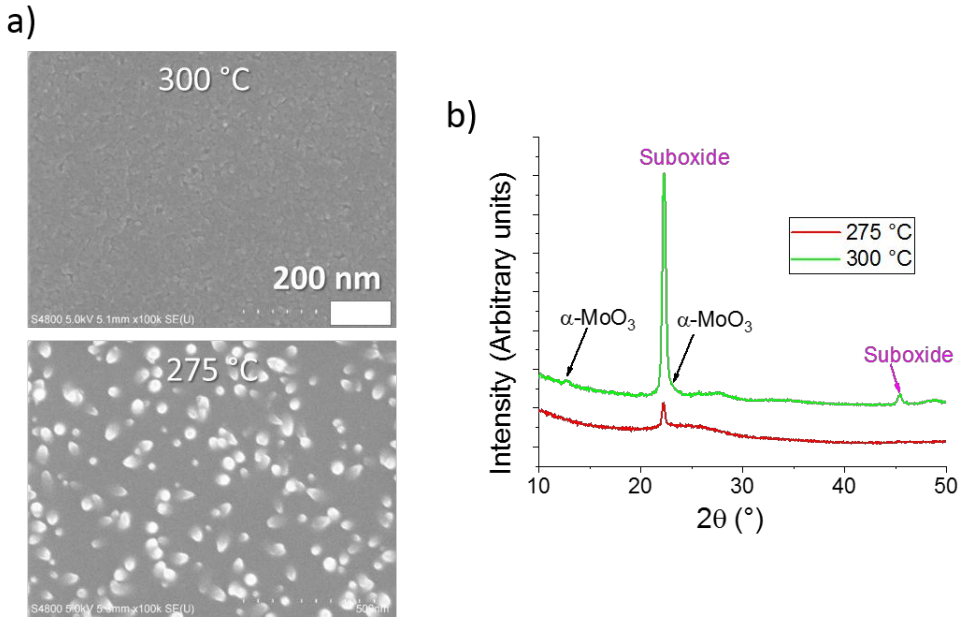

Figure S27 a) SEM images and b) grazing incidence X-ray diffractograms of 50 nm MoO_x films deposited at 275 and 300 °C.

References

(1) Nazri, G.; Julien, C. Far-Infrared and Raman Studies of Orthorhombic MoO_3 Single Crystal. *Solid State Ionics* **1992**, *53–56*, 376–382.

(2) Seguin, L.; Figlarz, M.; Cavagnat, R.; Lassègues, J.-C. Infrared and Raman Spectra of MoO_3 Molybdenum Trioxides and $MoO_3 \times H_2O$ Molybdenum Trioxide Hydrates. *Spectrochim. Acta Part A* **1995**, *51*, 1323–1344.

(3) Py, M. A.; Maschke, K. Intra- and Interlayer Contributions to the Lattice Vibrations in MoO_3. *Phys. B* **1981**, *105*, 370–374.

(4) McEvoy, T. M.; Stevenson, K. J. Spatially Resolved Imaging of Inhomogeneous Charge Transfer Behavior in Polymorphous Molybdenum Oxide. I. Correlation of Localized Structural, Electronic, and Chemical Properties Using Conductive Probe Atomic Force Microscopy and Raman Microprobe Spectros. *Langmuir* **2005**, *21*, 3521–3528.

(5) McCarron, E. M. β-MoO_3: A Metastable Analogue of WO_3. *J. Chem. Soc.* **1986**, *101*, 336–338.

(6) Dieterle, M.; Mestl, G. Raman Spectroscopy of Molybdenum Oxides. Part II. Resonance Raman Spectroscopic Characteriation of the Molybdenum Oxides Mo_4O_{11} and MoO_2. *Phys. Chem. Chem. Phys.* **2002**, *4*, 822–826.

(7) Olson, K. Laser Photodeposition of Molybdenum Oxide Thin Films from Organometallic Precursors (PhD Thesis), Iowa State University, 1989.

(8) Blume, A. Synthese Und Strukturelle Untersuchungen von Molybdän- Vanadium-, Und Wolfraoxide Als Referenzverbindungen Fur Die Heterogene Katalyse (PhD Thesis), TU Berlin, 2004.

(9) Ajito, K.; Nagahara, L. A.; Tryk, D. A.; Hashimoto, K.; Fujishima, A. Study of the Photochromic Properties of Amorphous MoO_3 Films Using Raman Microscopy. *J. Phys. Chem* **1995**, *99*, 16383–16388.

(10) Daniel, M. F.; Desbat, B.; Lassegues, J. C.; Gerand, B.; Figlarz, M. Infrared and Raman Study of WO_3 Tungsten Trioxides and $WO_3 \times H_2O$ Tungsten Trioxide Hydrates. *J. Solid State Chem.* **1987**, *67*, 235–247.

(11) Garcia-Sanchez, R. F.; Ahmido, T.; Casimir, D.; Baliga, S.; Misra, P. Thermal Effects Associated with the Raman Spectroscopy of WO_3 Gas-Sensor Materials. *J. Phys. Chem. A* **2013**, *117*, 13825–13831.